Effects of groundwater seepage in steady-state conditions in deep tunnel shafts

Norma P. López-Acosta, Gabriel Auvinet & Marco A. Pérez
Instituto de Ingeniería, UNAM, México.

2011 Pan-Am CGS Geotechnical Conference

ABSTRACT
The aim of this paper is to study the effects of groundwater seepage in steady-state conditions in the excavation of a 12m diameter and 90m deep tunnel shaft. Several of the soil strata located in the excavation area of the tunnel shaft are constituted by medium to high hydraulic conductivity materials, which generate important flow velocities and flow rates. Additionally, the presence of lower hydraulic conductivity strata interbedded between more permeable layers suggests the occurrence of significant hydraulic gradients, and therefore assessment of the uplift pressure in certain stages of the tunnel shaft excavation becomes necessary. A methodology to carry out this type of analyses by two-dimensional numerical modeling based on the finite element method is exposed. The results presented refer to the hydraulic head field, velocity vectors, among others, with emphasis on exit hydraulic gradients and flow rate at different stages of the tunnel shaft excavation. In particular, graphs related to the exit hydraulic gradient, exit seepage velocity, and flow rate as a function of the excavation depth are provided. Finally, conclusions of the analyses performed and recommendations in order to control the groundwater seepage and to mitigate uplift problems into the tunnel shaft are provided.

RÉSUMÉ
Le but de cet article est d'étudier les effets d'écoulement des eaux souterraines en régime permanent dans l'excavation d'un puits de 12m de diamètre et 90m de profondeur. Plusieurs strates du sol situé dans la zone d'excavation du puits sont constituées par des matériaux à moyenne et haute conductivité hydraulique, qui génèrent des vitesses d'écoulement et des débits importants. En outre, la présence de strates moins perméables intercalées entre des strates très perméables conduit à d'importants gradients hydrauliques, et par conséquent l'évaluation de la sous-pression dans certaines étapes d'excavation du puits devient indispensable. On expose une méthodologie pour effectuer ce type d'analyses par modélisation numérique à deux dimensions basée sur la méthode des éléments finis. Les résultats présentés se rapportent au domaine de la charge hydraulique, vecteurs de vitesse, entre autres, en mettant l'accent sur des gradients de sortie hydraulique et le débit à différentes étapes de l'excavation du puits. En particulier, on présente des graphiques liés au gradient de sortie hydraulique, vitesse de sortie et débit en fonction de la profondeur d'excavation. Enfin, on présente les conclusions des analyses effectuées et des recommandations en vue de contrôler l'écoulement des eaux souterraines et atténuer les problèmes de sous-pression dans le puits.

1 INTRODUCTION

The aim of this paper is to show the importance of performing groundwater seepage analyses through soils in geotechnical engineering practice projects. This type of analyses is not usually carried out, not even in projects of great geotechnical importance.

The tunnel shaft analyzed in this work is part of a deep drainage system. The study of this structure was chosen firstly because it is a tunnel shaft of a great depth (90m), this feature will cause a great hydraulic head loss between the original water table and groundwater level at the bottom of the excavation, which will generate important hydraulic gradients and seepage forces; and secondly, because this tunnel shaft is located in a very heterogeneous layered medium with contrasting hydraulic conductivities from one layer to another, which will cause variations in velocities, hydraulic gradients and flow rates in different stages of the tunnel shaft excavation.

Based on the aforesaid, this paper focuses on evaluating the results calculated by steady-state flow analyses in different stages of a tunnel shaft excavation. These results are related to the distribution of hydraulic potential or hydraulic heads, velocities, pore pressure, degree of saturation, among others, with emphasis on exit hydraulic gradients and flow rate in the tunnel shaft excavation. The stability of the bottom of the excavation due to uplift pressure is also assessed. Finally, conclusions and recommendations in order to control groundwater flow toward the tunnel shaft excavation and prevent the failure at the bottom of the excavation because of the uplift are provided.

2 FUNDAMENTALS OF THE STEADY-STATE FLOW ANALYSIS

Analyses of two-dimensional steady-state groundwater seepage are governed by the following partial differential equation:

$$k_x \frac{\partial^2 h}{\partial x^2} + k_y \frac{\partial^2 h}{\partial y^2} = 0 \qquad [1]$$

Where k_x and k_y are hydraulic conductivities of soil in X and Y directions, respectively, and h is hydraulic potential or hydraulic head. When soil is homogeneous and isotropic, Equation 1 is named *Laplace's equation*.

This equation is established based on continuity of flow equation, and with Darcy's law given by:

$$V_x = -k_x \frac{\partial h}{\partial x} \quad ; \quad V_y = -k_y \frac{\partial h}{\partial y} \qquad [2]$$

Where $\partial h/\partial x$ and $\partial h/\partial y$ are hydraulic gradients in *X* and *Y* directions, respectively (they are defined as hydraulic head loss per unit length). Besides, seepage force per unit volume is given by:

$$j = i\gamma_w \qquad [3]$$

Where *i* is the hydraulic gradient and γ_w is the unit or volumetric weight of water.

Additionally, the total hydraulic head at any point of the flow domain is simply:

$$h = y + \frac{P}{\gamma_w} \qquad [4]$$

Where *y* is the position head and P/γ_w is the pressure head (in addition *P* is the pore pressure).

Different techniques to solve Equation 1 can be applied: exact or approximate methods, analytical or numerical methods (Harr 1962; Cedergren 1967; Reséndiz 1983; López and Auvinet 1998; Flores 1999; among others). In general, exact and analytical solutions are laborious when geometric, hydraulic and boundary conditions are complex. In these situations it is frequent to use approximate solutions. Among several techniques, numerical methods are the most common, they include finite element and finite differences methods, whose use has become recurrent in recent decades due to its easy adaptation and automation of widely varying conditions, and in general due to their ability to solve complex problems. In this paper a specialized computer program that allows performing analyses based on finite element method is used (2D PLAXFLOW V1.5; DELFT Netherlands 2007). The methodology to perform 2D steady-state flow analyses by the previous algorithm is illustrated in Figure 1.

n what follows, the application of finite element method by using *Plaxflow* algorithm for the study of groundwater seepage in the excavation of a very deep tunnel shaft is shown.

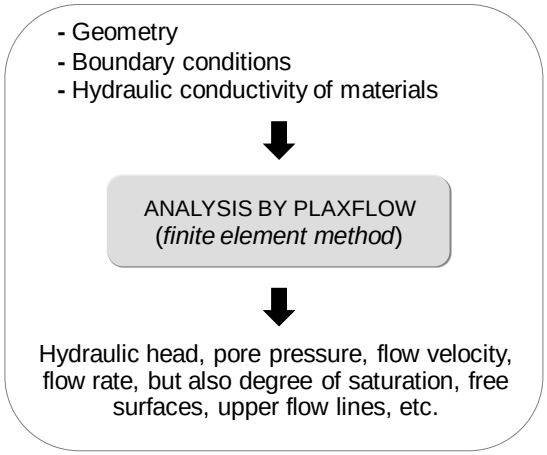

Figure 1. Steady-state analysis using *Plaxflow* algorithm

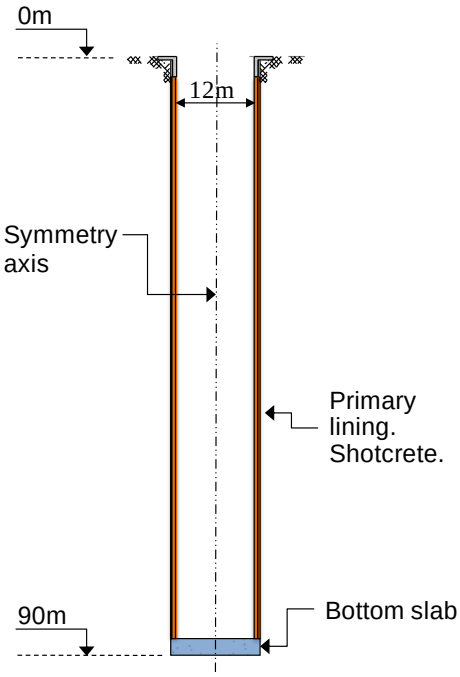

Figure 2. Cross section of the analyzed tunnel shaft excavation.

3 APLICATION TO A DEEP TUNNEL SHAFT

3.1 Geometric, hydraulic and boundary conditions

The steady-state seepage in different stages of the conventional excavation of the 90m deep and 12m diameter tunnel shaft illustrated in Figure 2 is analyzed.

The depth of the 27 excavation stages considered in the analyses are those listed in Table 1 (they are schematically shown in Fig. 3).

The existence of an important number of interbedded strata with different hydraulic conductivities is the main characteristic of subsoil where the studied tunnel shaft is excavated. The simplified soil profile and hydraulic conductivities of materials existing in the domain of interest are shown in Figure 3. In this paper, subsoil strata are assumed to be homogeneous and isotropic (k_x=k_y).

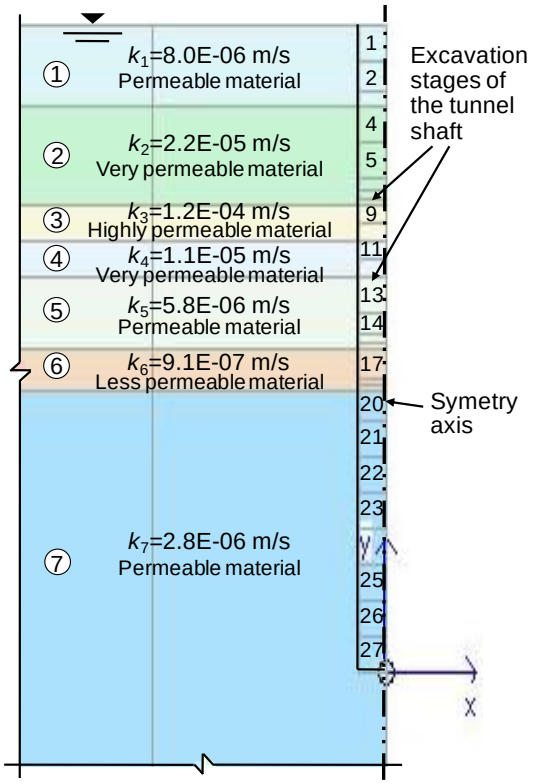

Figure 3. Simplified soil profile and hydraulic conductivities of studied domain materials.

Analyses are performed considering only half a cross section of the tunnel shaft due to symmetry of the flow problem. The simplified geometry and the finite element mesh used for modeling the domain of interest are illustrated in Figure 4. It refers to a two-dimensional mesh constituted by 5718 triangular elements (three nodes coinciding with the vertices of the triangle) and a total of 2959 nodes.

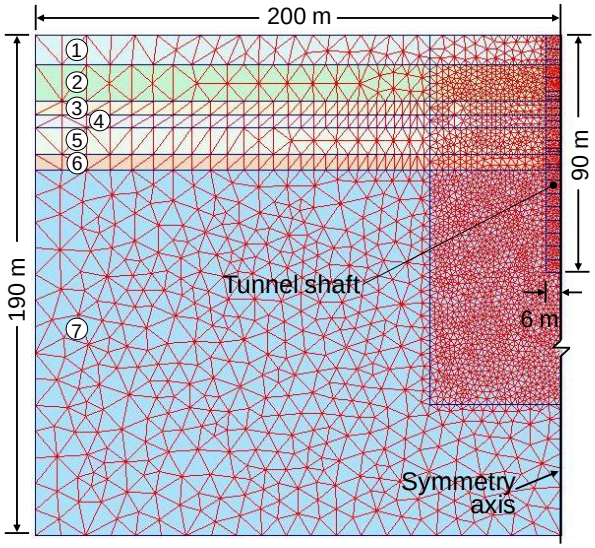

Figure 4. Simplified geometry and finite element mesh in the domain of interest.

Similarly, general boundary conditions considered in analyses are shown in Figure 5. In this figure, boundary equipotential lines (with imposed hydraulic head) correspond to *permeable boundaries*, and boundary flow lines represent *impermeable boundaries.* On the other hand, the primary lining of the tunnel shaft is assumed to be an impermeable boundary. It must be remarked that analyses were performed considering the most critical condition that can occur *in situ*, namely when the water level (W.L.) is located on the natural ground level.

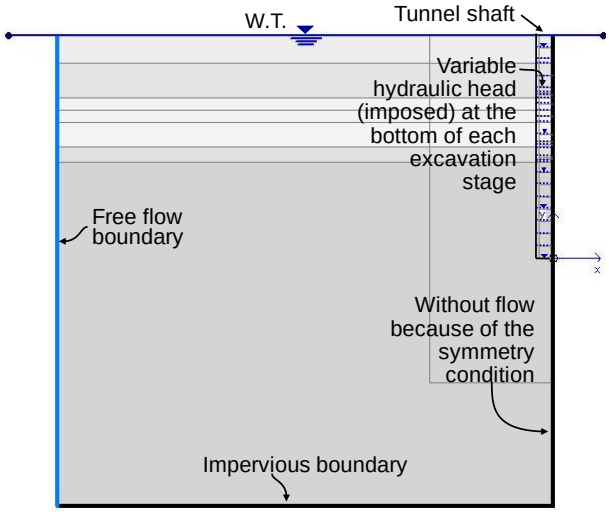

Figure 5. Boundary conditions assumed in calculations.

3.2 Results and discussion

Hydraulic head field and pore pressure field in one of the excavation stage of the tunnel shaft (excavation 17) obtained from the analysis are presented in Figures 6 and 7, respectively. These preceding resulting fields are modified for each stage of excavation, mainly in the area near the excavation. Additionally, the degree of saturation in the flow domain also for excavation stage 17 is shown in Figure 8.

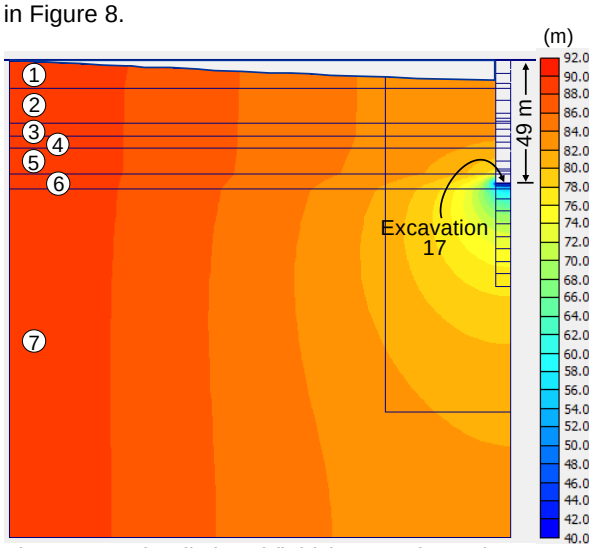

Figure 6. Hydraulic head field (Excavation 17).

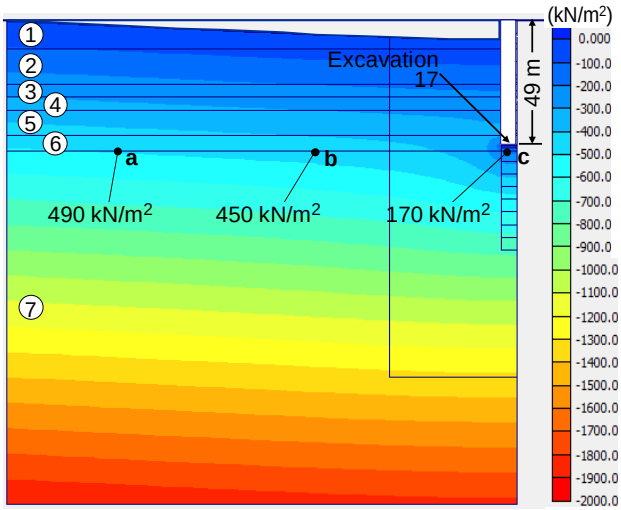

Figure 7. Pore pressure field (Excavation 17).

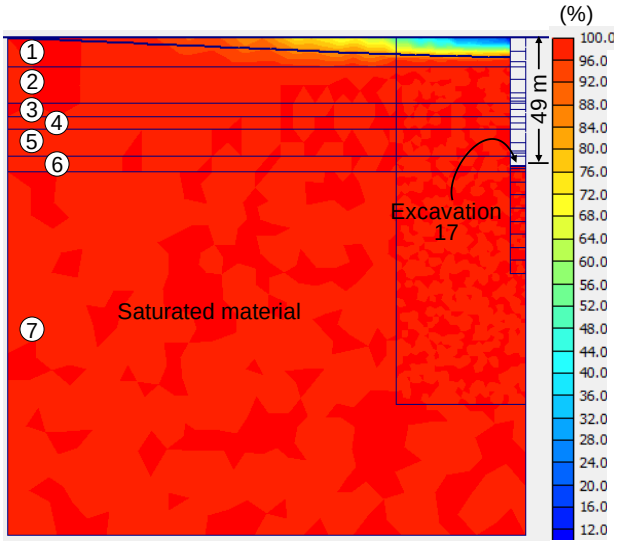

Figure 8. Degree of saturation in the studied domain (Excavation 17).

On the other hand, if each tunnel shaft excavation was constructed in the same subsoil material, then seepage velocities, hydraulic gradients and flow rates at the bottom of the excavation would tend to increase with increasing deep of the excavation; this occurs due to the increment on hydraulic head loss (higher difference between the original water table and the groundwater level at the bottom of each excavation). However, due to the existence of materials with different hydraulic conductivities in the subsoil of interest (Fig. 3), seepage velocities, hydraulic gradients and total flow rate at the bottom of each excavation exhibit variations depending on material where excavation is located. Variation of upward exit velocity as a function of the excavation depth is shown in Figure 9. The resulting point values are listed in detail in Table 1. These results show that the highest upward exit velocity ($V_{máx}$ = 1.54×10^{-5} m/s) is reached at a depth of 24m (in excavation 17), just before the excavation crosses the most permeable stratum of the analyzed flow domain (material 3, see Fig. 3). The results for stages 5 and 9 in Figure 10 demonstrate how the water tends to move through the referred material 3. Once the depth of the excavation crosses material 3, velocity vectors magnitude tends to decrease as illustrated in stages 20 and 27 of Figure 10.

Figure 11 illustrates that contrary to flow velocity, higher exit hydraulic gradients i_s at the bottom of the excavation occur when excavation reaches the less permeable material of the analyzed flow region (material 6, Fig 3), that is in excavations 17 and 18 (at a depth of 49m and 50m, respectively). Because the seepage force per unit volume is equal to the hydraulic gradient multiplied by the volumetric weight of water γ_w (Eq. 3), the above comments have a direct impact on the uplift pressure acting on the bottom of the excavation at these depths (starting from 49m). The particular values of the exit hydraulic gradient obtained in different stages of the tunnel shaft excavation are listed in Table 2.

Figure 12 illustrates flow rates obtained for each excavation. In this case, the higher flow rate ($q_{máx}$ = 1.74×10^{-3} m^3/s) is obtained when the higher exit velocity is reached (in excavation 7, at a depth of 24m), just before the excavation crosses the most permeable stratum of the analyzed flow domain (material 3). The particular values of flow rates for each excavation stage are provided in Table 3. These values were computed considering a 12m average perimeter value of the tunnel shaft (as indicated in Fig. 2).

3.3 Assessment of the uplift pressure

Serious problems may be provoked by the pore pressure acting on the base of a continuous relatively impervious layer located beneath the bottom of an excavation. The seepage toward the excavation lowers the piezometric level of only the body of water located above the relatively impervious layer, whereas that below this stratum remains unchanged (Terzaghi and Peck 1967).

Thus, taking into account maximum hydraulic gradients obtained in analyses performed here, the uplift in stage 17 of the tunnel shaft excavation is assessed according to data illustrated in Figure 13. In this case, the pressure on the base of material 6 due to the weight of the overlying soil (and located beneath the bottom of the excavation 17) is:

$$\gamma_m L = 17.5\,kN/m^3 \quad 2m \quad = 35\,kN/m^2 \qquad [5]$$

The upward pore pressure on the base of material 6, which is computed by using *Plaxflow* algorithm (see point 'c' in Fig. 7) is:

$$u \approx 170\,kN/m^2 \qquad [6]$$

If the upward pore pressure u is greater than the weight of the overlying soil $\gamma_m L$, the bottom of the excavation rises generating uplift failure, as in this case:

$$170\,kN/m^2 > 35\,kN/m^2 \qquad [7]$$

The minimum thickness L_i of the layer of interest that should be considered to ensure stability of the bottom of the excavation is (defined in the local building code; NTCDCC 2004):

$$L_i > \left(\frac{\gamma_w}{\gamma_m}\right) h_w \qquad [8]$$

Where h_w is the piezometric hydraulic head at the lower part of the impermeable layer; γ_w is the volumetric weight of water; γ_m is the total volumetric weight of soil between the bottom of the excavation and the permeable stratum. Thus, in this case a thickness of L_i =10m in material 6 would be required for avoiding uplift failure.

Additionally, results given in Table 4 demonstrate that there is no uplift problems before excavation 17 of the tunnel shaft (49m depth).

Table 1. Exit velocity in each excavation stage.

Excavation N°	Excavation depth, *z* (m)	Exit velocity *V* (m/s)
0	0.0	0.00
1	5.0	2.09E-06
2	9.0	4.38E-06
3	11.0	6.43E-06
4	16.0	8.63E-06
5	21.0	1.18E-05
6	23.0	1.38E-05
7	24.0	1.54E-05
8	25.0	1.40E-05
9	27.5	9.95E-06
10	30.0	4.13E-06
11	32.5	7.64E-06
12	35.0	6.96E-06
13	40.0	6.72E-06
14	43.0	5.12E-06
15	44.0	3.94E-06
16	45.0	3.64E-06
17	49.0	6.23E-06
18	50.0	7.38E-06
19	51.0	8.27E-06
20	55.0	7.58E-06
21	60.0	8.01E-06
22	65.0	8.71E-06
23	70.0	8.99E-06
24	75.0	9.83E-06
25	80.0	1.01E-05
26	85.0	1.07E-05
27	90.0	1.05E-05

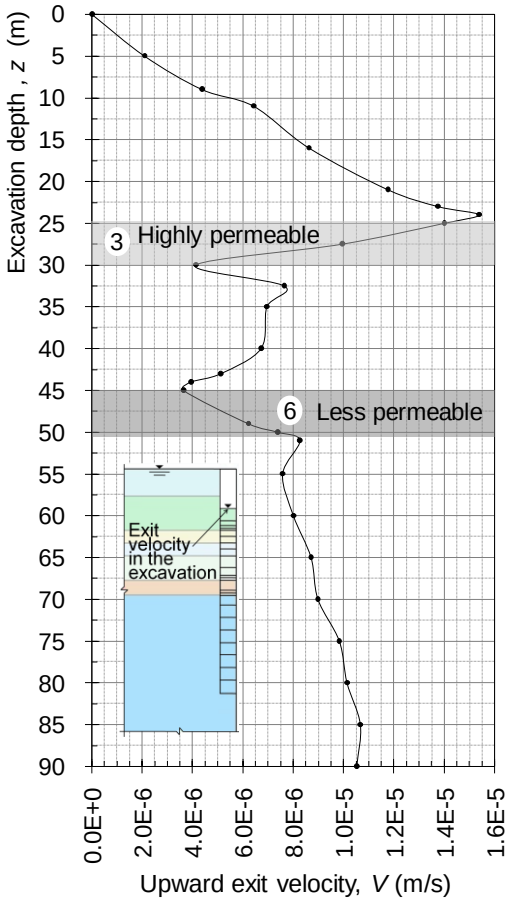

Figure 9. Upward exit velocity at the bottom of the excavation as a function of excavation depth.

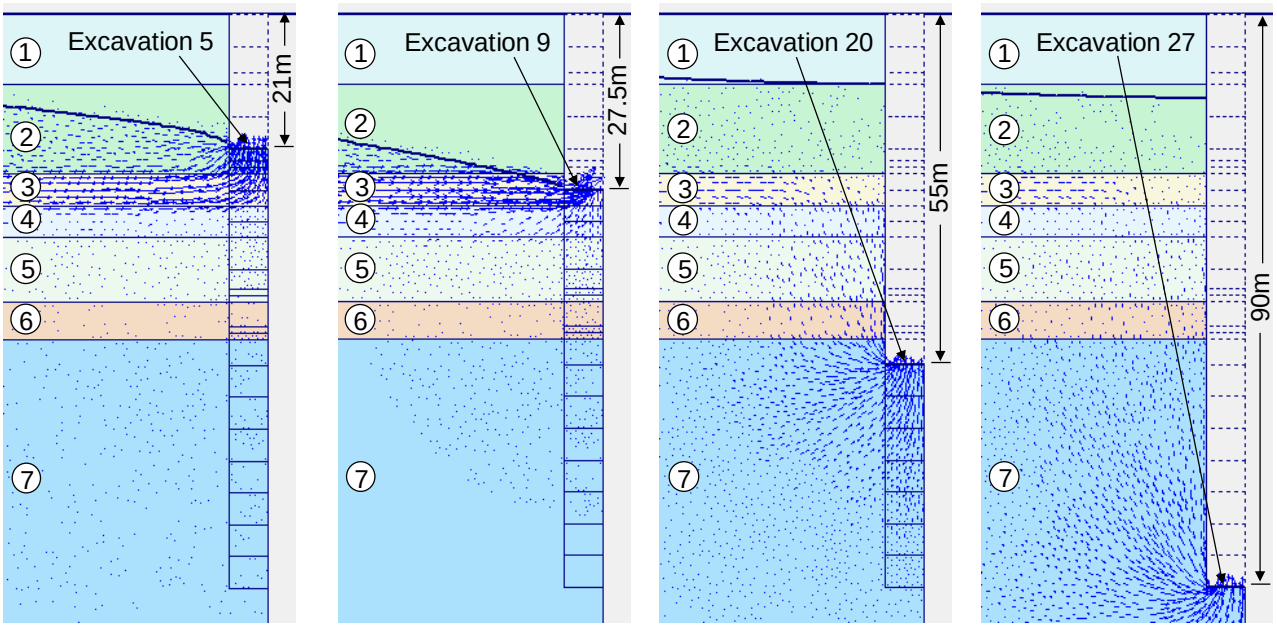

Figure 10. Velocity vectors (magnitude) for different excavation stages of the tunnel shaft.

Table 2. Exit gradient in each excavation stage.

Excavation N°	Excavation depth, z (m)	Exit gradient, i_s (dimensionless)
0	0.0	0.00
1	5.0	0.26
2	9.0	0.55
3	11.0	0.29
4	16.0	0.39
5	21.0	0.54
6	23.0	0.63
7	24.0	0.70
8	25.0	0.12
9	27.5	0.08
10	30.0	0.37
11	32.5	0.68
12	35.0	1.20
13	40.0	1.16
14	43.0	0.88
15	44.0	0.68
16	45.0	3.99
17	49.0	6.82
18	50.0	8.09
19	51.0	2.92
20	55.0	2.68
21	60.0	2.83
22	65.0	3.08
23	70.0	3.17
24	75.0	3.47
25	80.0	3.58
26	85.0	3.77
27	90.0	3.72

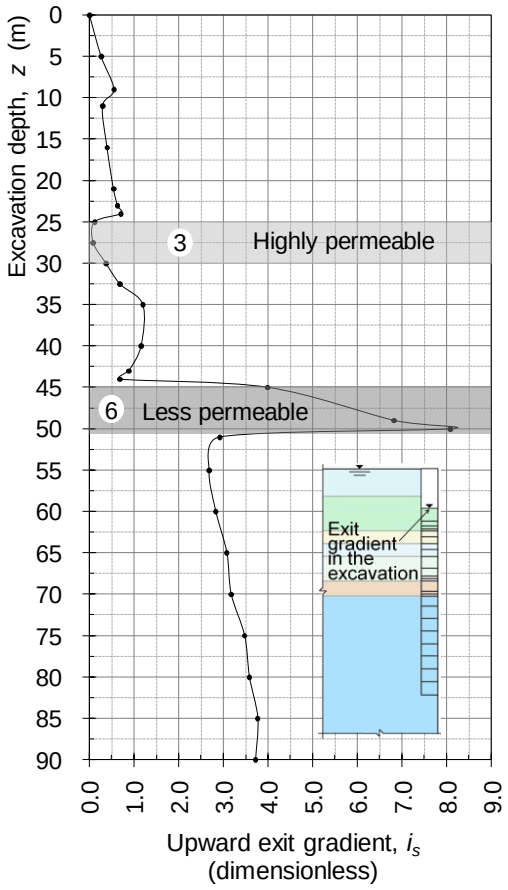

Figure 11. Exit gradient at the bottom of the excavation as a function of excavation depth.

Table 3. Flow rate in each excavation stage.

Excavation N°	Excavation depth, z (m)	Flow rate q_t (m^3/s)
0	0.0	0.00
1	5.0	2.37E-04
2	9.0	4.95E-04
3	11.0	7.28E-04
4	16.0	9.76E-04
5	21.0	1.33E-03
6	23.0	1.56E-03
7	24.0	1.74E-03
8	25.0	1.59E-03
9	27.5	1.12E-03
10	30.0	4.67E-04
11	32.5	8.64E-04
12	35.0	7.87E-04
13	40.0	7.60E-04
14	43.0	5.79E-04
15	44.0	4.46E-04
16	45.0	4.12E-04
17	49.0	7.04E-04
18	50.0	8.35E-04
19	51.0	9.35E-04
20	55.0	8.57E-04
21	60.0	9.06E-04
22	65.0	9.85E-04
23	70.0	1.02E-03
24	75.0	1.11E-03
25	80.0	1.15E-03
26	85.0	1.21E-03
27	90.0	1.19E-03

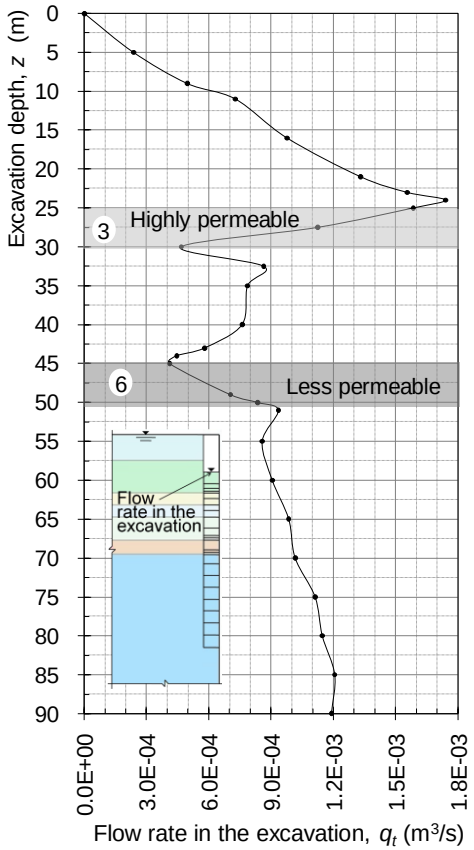

Figure 12. Flow rate in each excavation stage.

Table 4. Calculations for the uplift analysis.

Excavation N°	Depth, z (m)		Volumetric weight of material	Pore pressure at 51m depth[1]	Vertical stress at 51m depth[1]
	From	To	γ_m (kN/m3)	u (kN/m^2)	σ_v (kN/m^2)
0	0.0	0.0		0.0	993.1
1	0.0	5.0	16.0	1.2	913.1
2	5.0	9.0		2.7	849.1
3	9.0	11.0		3.7	817.1
4	11.0	13.0	17.0	5.8	725.2
	13.0	16.0	19.3		
5	16.0	17.0		8.5	596.7
	17.0	21.0	27.3		
6	21.0	23.0		9.9	542.1
7	23.0	24.0		10.6	514.8
8	24.0	25.0		11.5	487.5
9	25.0	27.5	17.5	13.0	443.8
10	27.5	30.0		12.1	400.0
11	30.0	32.5	17.0	14.2	357.5
12	32.5	35.0		17.0	315.0
13	35.0	40.0	17.0	32.5	230.0
14	40.0	43.0	25.0	41.9	155.0
15	43.0	44.0		37.9	130.0
16	44.0	45.0		41.3	105.0
17	45.0	49.0	17.5	116.4	35.0
18	49.0	50.0		146.7	17.5
19	50.0	51.0		175.2	0.0

[1]As a function of excavation depth.

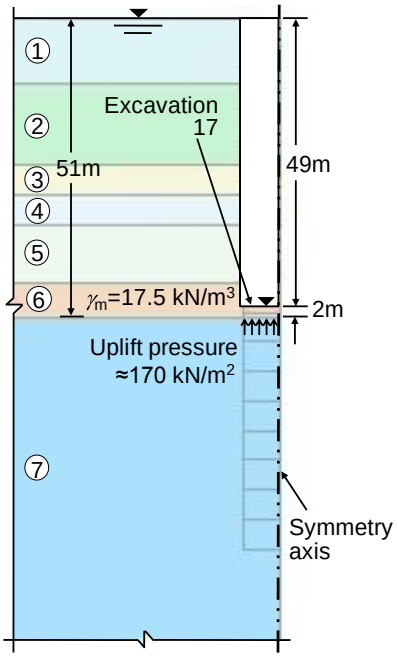

Figure 13. Uplift pressure in excavation 17.

3.4 Additional calculations and recommendations

As distinguished in the preceding paragraphs, there are two principal problems that must be faced in the excavation of the analyzed tunnel shaft:

- Large flow velocities and significant groundwater filtrations before crossing the most permeable layer of the flow region (see material 3 in Fig. 3), mainly between depths of 20 to 25m.
- Large hydraulic gradients and therefore, uplift problems starting from stage 17 of the excavation (49m depth).

Several additional calculations were performed considering some structures helping to correct or mitigate the aforementioned problems.

In this way, in order to control groundwater filtrations toward excavation, the installation of a pumping well with 2 l/s of extraction rate located in material 3 (29m depth) is proposed, as illustrated in Figure 14.

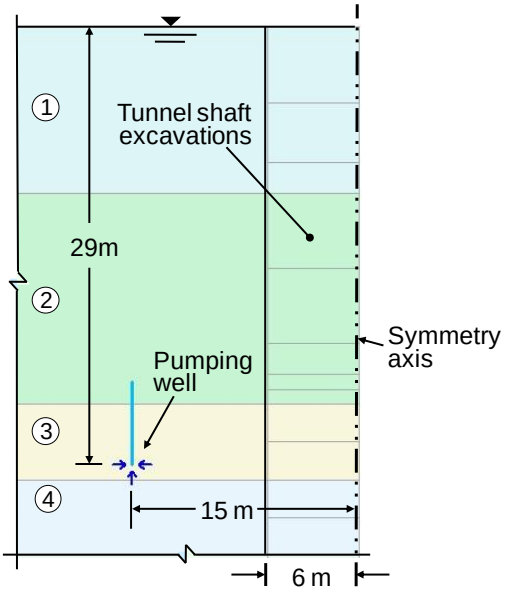

Figure 14. Installation of a pumping well in material 3 of the flow region.

Taking into account the existence of this pumping well, Figure 15 indicates how degree of saturation varies since initial excavation stage of the tunnel shaft in comparison with the case where the pumping well is not installed (see Fig. 8). Comparing Figures 8 and 15, it can be clearly appreciated how the unsaturated material region increases due to the presence of the pumping well. The influence area reaches approximately the bottom part of material 6 (at a depth of 51m) as shown in Figure 15. However, beyond this material 6 (after excavation 17), the presence of the pumping well has no significant influence on results, as observed in Figure 16. This fact can be better distinguished observing velocity vectors in Figure 17, in which the velocity vectors relating to excavations 5 and 9 confirm the watertightness at the bottom of the tunnel shaft with the operation of the well; instead, the velocity vectors relating to excavations 17 and 27 continue exhibiting the uplift problem beneath material 6.

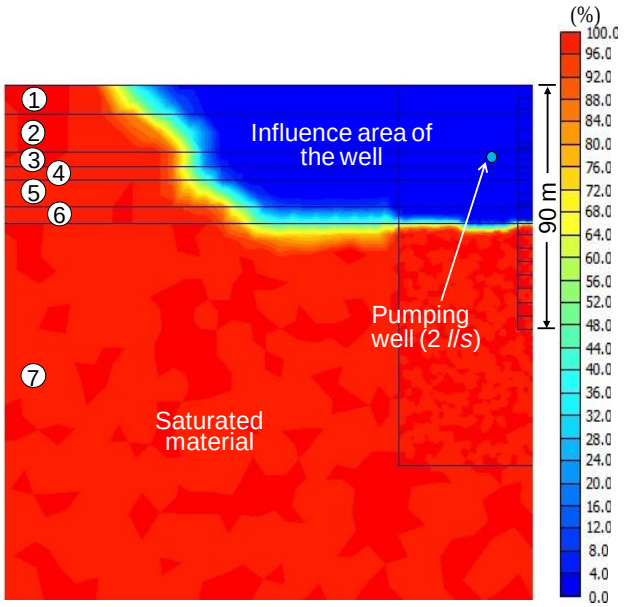

Figure 15. Degree of saturation in the initial stage of excavation (considering a pumping well).

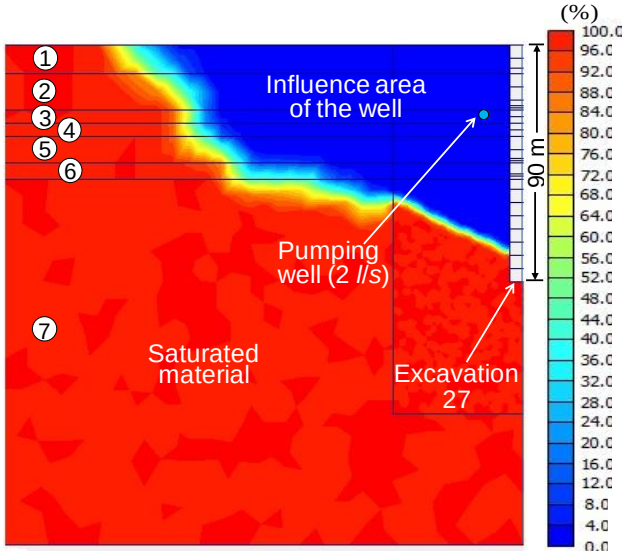

Figure 16. Degree of saturation in stage 27 of excavation (considering a pumping well).

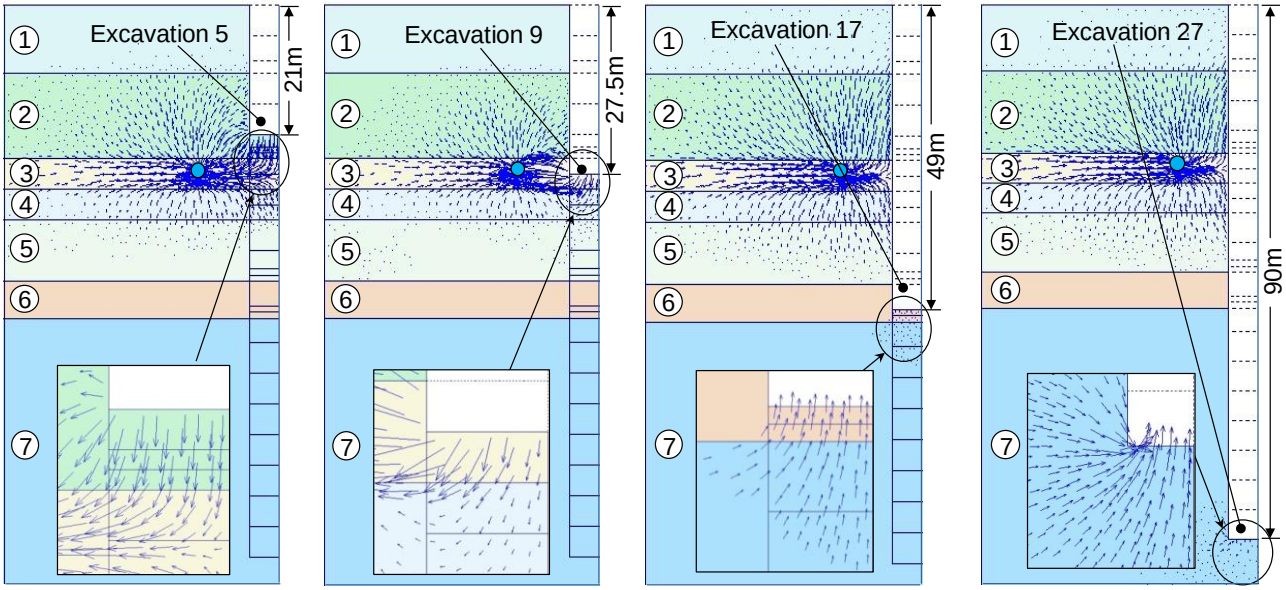

Figure 17. Velocity vectors (magnitude) for different excavation stages of the tunnel shaft, considering the installation of a pumping well.

Based on prior results, in order to correct the uplift problem below material 6, we propose the construction of three relief wells according to the location and dimensions indicated in Figure 18. It is suggested that these relief wells are constructed as the excavation progresses. The purpose is to avoid the significant pore pressure that would be reached at the bottom of the tunnel shaft if a single relief well was constructed up to the final depth of the tunnel shaft (90m).

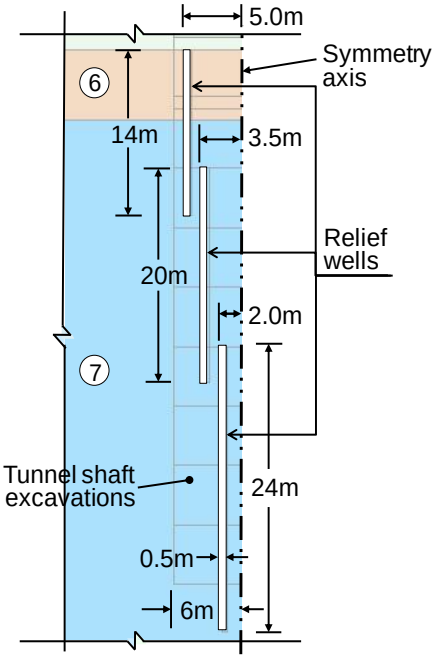

Figure 18. Installation of relief wells starting from material 6 (45m depth).

The usefulness of these relief wells can be appreciated in the change of direction or reduction of velocity vectors in excavations 17 and 27 of Figure 19, compared with velocity vectors obtained in the same stages but for the case in which relief wells are not considered (Fig. 17).

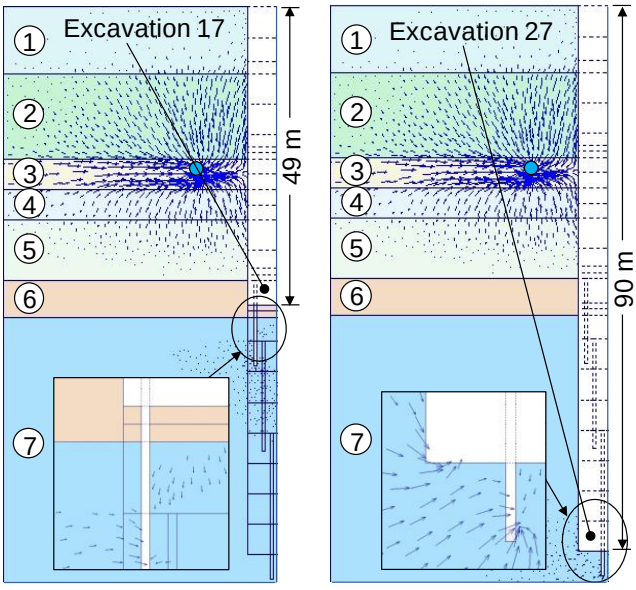

Figure 19. Velocity vectors (magnitude) for different stages of the tunnel shaft excavation, considering relief wells constructed starting from material 6 (45m depth).

4 CONCLUDING REMARKS

Steady-state flow analyses in the excavation stages of a 12m diameter and 90m depth tunnel shaft by two-dimensional numerical modeling based on finite element method were performed.

According to results of analyses, two predominant problems from a hydraulic point of view were distinguished:

- The most permeable stratum of the flow region (material 3) generates significant groundwater filtrations (1.7 l/s approximately), mainly between depths from 20m to 25m.
- On the contrary, the most impermeable stratum of the flow region (material 6) causes uplift problems starting from 49m depth.

Additional calculations performed in order to correct the previous problems allowed establishing that:

- The groundwater filtrations at the bottom of the tunnel shaft excavation can be mitigated by the installation of a pumping well in material 3 of the analyzed domain (29m depth and 2 l/s extraction rate).
- On the other hand, the uplift problems can be mitigated by the construction of relief wells in the most impermeable stratum of the studied domain (starting from 45m depth).

The abovementioned results demonstrate the utility of these simple numerical evaluations in solutions of geotechnical engineering practice problems.

5 REFERENCES

Cedergren, H. R. 1967. *Seepage, drainage and flow nets*, Third edition, John Wiley and Sons.

Flores, R. 1999. *Flow of water through soils,* Advances in Hydraulics 4, Mexican Association of Hydraulics and Mexican Institute of Water Technology (IMTA), Cuernavaca, Mexico (in Spanish).

Harr, M. E. 1962. *Groundwater and seepage*, Dover Publications INC.

López, N. P. and Auvinet, G. 1998. Groundwater seepage in soils with random permeability, *Proceedings of the XIX National Meeting of Soil Mechanics*, SMMS, Session 7: 404-411 (in Spanish).

NTCDCC. 2004. Complementary Technical Standards for Design and Construction of Foundations. Mexican City Building Code, GDF (October 6, 2004) (in Spanish).

PLAXIS VB, 2007, PLAXFLOW 2D V1.5. Finite Element Code for steady-state and transient flow. Scientific Manual, Edited by Brinkgreve, R.B.J., DELFT University of Technology & Plaxis. The Netherlands.

Reséndiz, D. 1983. *Flow of water. Methods of analysis*, Part B, Chapter 5, Book title: Earth and rockfill dams. Edited by Marsal, R. J. and Reséndiz, D., Limusa, Mexico.

Terzaghi, K. and Peck, R. B. 1967. *Soil mechanics in engineering practice*, 2nd ed., John Wiley and Sons Inc.